*Journal of Power Sources*, 45 (1993) 195–207



# Lightweight nickel electrodes for nickel/hydrogen cells

Hong S. Lim and Gabriela R. Zelter
*Industrial Electronics Group of Hughes Aircraft Company, P.O. Box 2999, Torrance, CA 90509-2999 (USA)*

(Received October 21, 1992; accepted in revised form January 28, 1993)

**Abstract**

Thick nickel electrodes with lightweight substrate material have been prepared and tested in $Ni/H_2$ boilerplate cells containing 26% KOH electrolyte. Lightweight substrates used in this study were either 85 or 90% in porosity and either 0.8 or 2 mm in thickness, respectively, compared with 80 to 82% porosity and 0.75 to 0.8 mm thickness of the state-of-the-art sintered plaque substrate. All of these thick electrodes had substantially improved theoretical (or chemical) capacity over that of state-of-the-art sintered nickel plaque electrodes. However, utilization of the active material was low (65 to 80%) compared with that of the state-of-the-art electrodes (approximately 90%) in 26% KOH. Due to this low utilization, the electrodes using 85% porous substrates did not show any advantage over the state-of-the-art ones. The electrodes using a 90% porous substrate, however, showed 17% higher usable specific capacity (about 0.13 Ah/g in 26% KOH) than that of the state-of-the-art nickel electrodes despite the low utilization. These electrodes achieved up to 4860 cycles at 40% depth-of-discharge with neither capacity loss nor any significant changes of rate capability and charging efficiency with cycling.

## Introduction

A lightweight long-life battery is desired as space power needs grow [1]. The $Ni/H_2$ cell is well known for its long cycle life [2, 3] and high reliability for space power application. Although the Ni/Cd battery is available as an alternate energy-storage device for long-life spacecraft, it is less attractive than the $Ni/H_2$ battery for high power spacecraft. Therefore, a $Ni/H_2$ battery with improved specific energy is highly desirable. The nickel electrode is the heaviest component of present $Ni/H_2$ cells and the nickel electrodes account for about one third of the cell weight. The weight of the sintered plaque substrate material is approximately 60% of the nickel electrode. Therefore, a high porosity (90%) plaque substrate material is very attractive compared with the state-of-the-art sintered nickel plaque (80 to 82% porous), because a 90% porous substrate material has only one half the weight of a state-of-the-art sintered plaque substrate. In addition, the use of fewer thick (e.g., 2 mm) nickel electrodes will reduce the number of separators, hydrogen electrodes, and other auxiliary components, and thereby further reduce total cell weight. Highly porous (85 to 90%) nickel plaque substrates made of 50% nickel powder and 50% nickel fiber are commercially available ('Fibrex' from National Standard Co.). Nickel electrodes made of these substrates are attractive for use in a lightweight $Ni/H_2$ cell [4]. High active material utilization (> 100%) was observed with thin electrodes made of 90% porous substrate after several hundred cycles in a cell flooded with 26% KOH electrolyte.

0378-7753/93/$6.00

This paper reports the results of performance and cycle-life tests of similar nickel electrodes using thick high porosity (85 to 90%) substrates in boilerplate Ni/$H_2$ cells. Results of initial and post-cycling characterizations and destructive physical analysis are also discussed.

## Experimental

*Nickel electrodes*

The electrode substrate material was of the sintered type having a composition of 50% Ni fiber, 40% Ni powder and 10% Co powder ('Fibrex' brand from National Standard Co.). A scanning electron micrograph (SEM) of this substrate material is shown in Fig. 1. Electrodes were prepared without coining plaque substrate and loaded with active material using an electrochemical impregnation technique in an aqueous ethanol bath [5]. Electrodes for A-type cells were prepared using substrate material which was nominally 0.8 mm thick and 85% porous. Those for B- and C-type cells were 2 mm thick, 85% porous while those for D-type cells were 2 mm thick but 90% porous. B- and C-type electrodes were identical except that C-type electrodes were loaded heavier than the B-type.

*Cell designs*

All test cells were demountable boilerplate cells similar to those used in our earlier studies [6, 7]. They were made of a heavy wall (1 inch thick) stainless-steel vessel. All cell stacks were in a back-to-back configuration as shown in Fig. 2 (A-type cells) and in Fig. 3 (B-, C- and D-type cells). All electrodes had the same dimensions as for the USAF/Hughes standard 3.5-inch diameter individual pressure vessel (IPV) cell [8]. A-type cells had two pairs of nickel electrodes. Other cells (B-, C- and D-

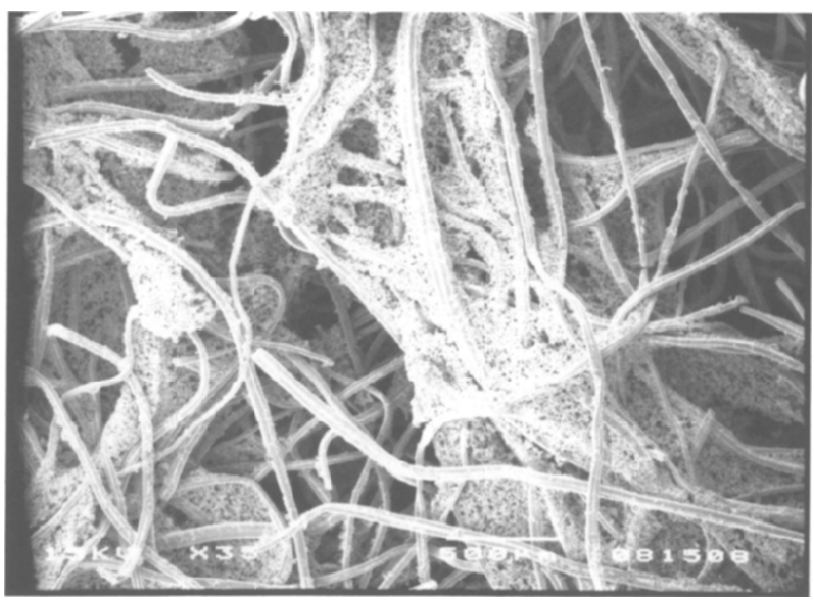

Fig. 1. SEM pictures of a 90% porous 'Fibrex'-sintered electrode substrate material.

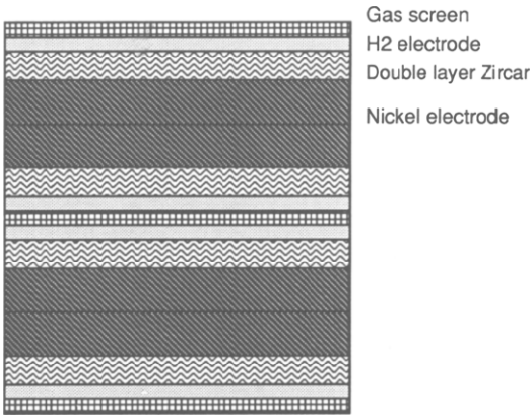


Fig. 2. Type A $Ni/H_2$ boilerplate cell stack design using 0.8 mm thick electrodes.

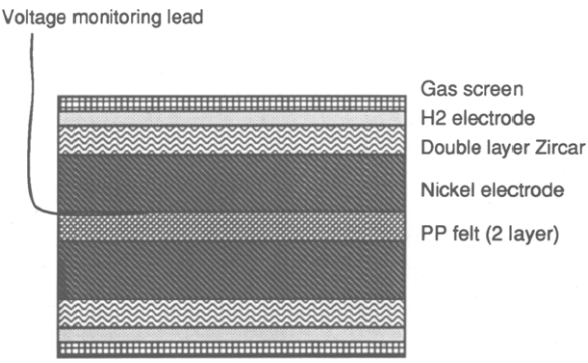


Fig. 3. Type B, C, and D $Ni/H_2$ boilerplate cell stack design using 2 mm thick electrodes.

types) had one pair of nickel electrodes with an electrolyte reservoir made of polypropylene (PP) felt. All cells were activated using 26% KOH electrolyte and had an excess amount of the electrolyte (approximately 10–20 ml) at the bottom of the pressure vessel. A-type cells were rated at 5.0 Ah and the other cells at 6.0 Ah.

*Performance and cycling tests*

A series of capacity measurements was carried out prior to cycling for initial characterization of the test cells. This characterization test involved measurements of cell capacity using various charge and discharge rates in order to evaluate the effects of the rates on the capacity. For the charge rate effect, cells were charged at *C*/10 rate for 18 h, *C*/2 rate for 160 min, or *C* rate for 80 min, respectively, followed by discharge at *C*/2 to 1.0 V and then to 0.5 V. For the discharge-rate effect, cells were charged at *C*/2 rate for 160 min followed by discharge at *C*/5, *C*/2, *C* or 2*C* rates, respectively, to 1.0 V and then to 0.5 V.

The low earth orbit type cycling tests were carried out at 40% depth-of-discharge of the rated capacity at 20 °C in an air-circulated constant temperature chamber. Cells were discharged at 0.69 *C* rate for 35 min followed by a 55 min charge at 0.46 *C* for 105% recharge. Test cells were cycled up to 4860 cycles. Interim capacities were

measured after 521 and 1600 cycles. For these measurements the cycling test was interrupted at the end of charge and then the cells were discharged at *C*/2 to 0.5 V. Subsequently, capacities were measured twice more by charging at *C*/2 for 160 min followed by discharging at *C*/2 to 0.5 V. After cycling, a post-cycling characterization test was carried out using a procedure similar to the initial characterization test.

*Destructive physical analysis*

Destructive physical analysis was carried out on all test cells. The analysis involved visual inspection of cell components during disassembly of the cell stack, measurements of nickel electrode expansion, SEM of the electrodes, chemical analyses, and electrode capacity measurements in flooded electrolyte cells. These cells were made of two nickel electrodes for A-type and one nickel electrode for B-, C- and D-type, respectively. The capacities were measured by cycling three times successively in 26% KOH, 31% KOH, and 36% KOH electrolytes, respectively. The cycling involved charging for 18 h at 0.30 A followed by discharging at 1.5 A to 0.5 V.

## Results and discussions

Nickel electrodes were prepared using plaque substrates of 85 and 90% in porosity and 0.8 and 2 mm in thickness, respectively. Active-material loading levels ranged from 1.54 to 1.75 g/cm$^3$ void. Electrode loading data and theoretical cell capacity data for individual electrodes are summarized in Table 1. The theoretical capacity was calculated from the electrode weight gain from active material impregnation under the assumption that all active material is $Ni(OH)_2$ and one electron transfers per nickel atom. This theoretical specific capacity value is substantially higher than that of the state-of-the-art electrodes (0.11 to 0.12 Ah/g). For example, average values for

TABLE 1

Electrode-loading data for boilerplate test cells

| Cell no. | Electrode thickness (mm) | Plaque porosity (%) | Average loading level (g/cm$^3$ void) | Theoretical specific capacity[a] (Ah/g) | Theoretical cell capacity[b] (Ah) |
|---|---|---|---|---|---|
| A1 | 0.810 | 85.5 | 1.59 | | 6.32 |
| A2 | 0.828 | 86.0 | 1.55 | | 6.32 |
| A3 | 0.805 | 85.7 | 1.58 | | 6.29 |
| B1 | 2.251 | 85.8 | 1.54 | 0.147 | 8.64 |
| B2 | 2.234 | 86.0 | 1.55 | 0.148 | 8.62 |
| B3 | 2.144 | 85.6 | 1.63 | 0.150 | 8.63 |
| C1 | 2.294 | 86.4 | 1.66 | 0.158 | 9.56 |
| C2 | 2.212 | 85.7 | 1.74 | 0.155 | 9.50 |
| C3 | 2.215 | 85.6 | 1.69 | 0.153 | 9.28 |
| D1 | 2.155 | 90.4 | 1.74 | 0.186 | 9.82 |
| D2 | 2.155 | 91.2 | 1.75 | 0.193 | 9.93 |
| D3 | 2.225 | 92.0 | 1.72 | 0.190 | 10.05 |

[a]Theoretical specific capacity of the state-of-the-art electrode is 0.11–0.12 Ah/g.
[b]Rated capacity of A1, A2, and A3 cells was 5 Ah and that of others was 6 Ah.

TABLE 2

Test cell history

| Cell | History |
|---|---|
| A1 | Failed after 2354 cycles |
| A2 | Failed after 2937 cycles |
| A3 | Failed after 2017 cycles |
| B1 | Failed after 2011 cycles |
| B2 | Failed after 2743 cycles |
| B3 | Developed short during initial capacity test |
| C1 | Failed after 2811 cycles |
| C2 | Failed after 1813 cycles |
| C3 | Removed after 4860 cycles |
| D1 | Removed after 4860 cycles |
| D2 | Removed after 4860 cycles |
| D3 | Removed after 4860 cycles |

B-type and D-type electrodes are 29 and 65% higher, respectively, than that of the state-of-the-art electrodes. These electrodes were tested for their initial performance characteristics and cycling behavior in a low earth orbit regime at 40% depth-of-discharge in $Ni/H_2$ boilerplate cells. The test history of individual cells is summarized in Table 2. All cells which failed in cycling had an abrupt failure indicating an internal short formation. The failed cells showed low end-of-discharge voltage (EODV) within a few cycles when they were recharged and put back into cycling, indicating that they had 'soft shorts'. Shorting was further indicated by the fact that the failed cells would not accept charge during subsequent interim capacity measurements. Because of these shorts, post-cycling characterization test results are available only for the four cells (C3, D1, D2, and D3) which did not fail in the cycling test. Reasons why these cells developed the shorts early in their life were not identified. However, it was speculated that use of uncoined electrodes might have caused shorts by an edge damage of nickel electrode by an overcharge either during cycle life test or activation. (B3 cell was shorted during activation.)

*Cycling test*

End-of-charge voltages (EOCV) and end-of-discharge voltage (EODV) of various type of cells are shown as a function of number of cycles in Fig. 4. End-of-charge pressure (EOCP) and end-of-discharge pressure (EODP) are shown in Fig. 5. The EODV, EOCP, and EODP gradually decreased with cycling. These decreases were found to be due to insufficient charging of the cells. Possible causes of this insufficient charging with 105% recharge, which is usually more than sufficient for a $Ni/H_2$ cell, may be due to either a high resistance soft short or deterioration of charge efficiency of the nickel electrodes. Changes of interim capacity values are shown as a function of number of cycles in Figs. 6 to 8 for various types of electrodes. With exception of the initial decrease of capacity with A-type cells and initial increase with C2 and D3 cells before 500 cycles, cell capacity values were stable throughout the cycles test for all cells. These stable capacity values indicate that the decrease in EODV, EOCP, and EODP with cycling is due to insufficient charging with 105% recharge ratio rather than due to capacity decrease with cycling as indicated by the result of post-cycling capacity measurements (Fig. 8) which did not show any decrease in capacity after

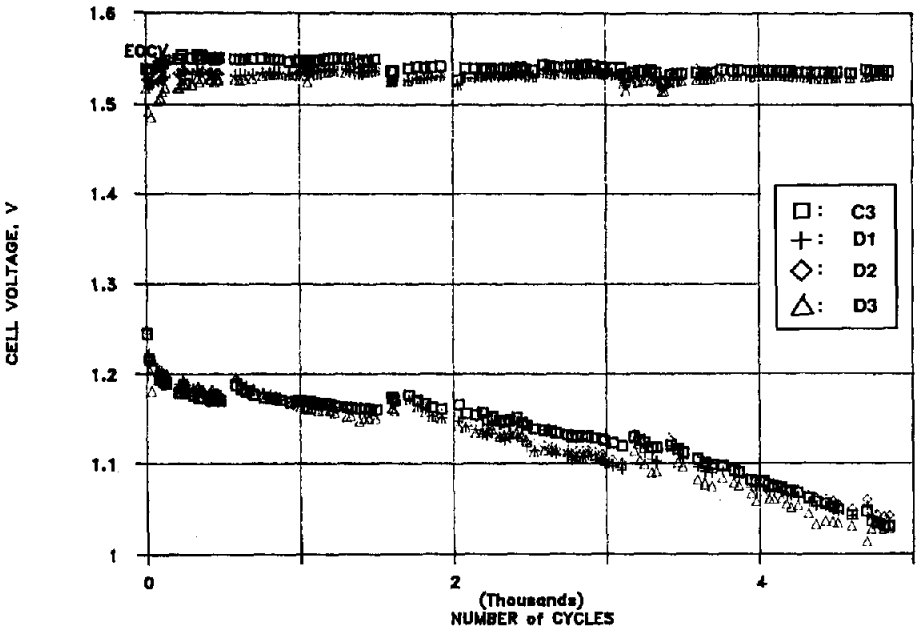


Fig. 4. Plots of end-of-charge voltages (EOCVs) and end-of-discharge voltages (EODVs) vs. number of cycles during the cycling test of C-type (85% porous) and D-type (90% porous electrodes): (□) C3; (+) D1; (◇) D2, and (△) D3.

4860 cycles. Utilization change of active material of A-type electrodes (85% porous 0.8 mm thick) is shown as a function of number of cycles in Fig. 9. The utilization was initially about 85% but decreased to 75 to 78% after 500 cycles. The utilization of B- and C-type electrodes (85% porosity, 2 mm thick) ranged between 65 to 71% which did not change significantly up to 1500 cycles. The utilization of C3 and all of D-type electrodes did not change significantly even after 4860 cycles (Fig. 10). Although the electrodes with the lightweight substrate had an attractive theoretical (chemical) specific capacity, the low utilization of the active material of these electrodes is a problem. Usable measured specific capacities of various types of electrodes are shown for comparison in Fig. 11. The usable capacity of those with 85% porous substrate (B- and C-types) was lower than or equal to that of a state-of-the-art sintered nickel electrode, thereby showing no merits over the state-of-the-art one. However, D-type electrodes have higher specific capacity (approximately 0.13 Ah/g) than the electrode with the state-of-the-art substrate (approximately 0.11 Ah/g).

*Initial and post-cycling capacity*

Initial and post-cycling characterization tests were carried out according to the procedure described in the experimental section. To illustrate the changes of the cell characteristics with cycling, the capacity values of four cells cycled for 4860 cycles are shown as a function of various charge rates and discharge rates, respectively, in Figs. 12 and 13. Typical discharge voltage curves at various discharge rates before and after the cycling test are shown in Fig. 14 and 15. There were no significant differences in charge accepting capability or discharge capability at high rates.

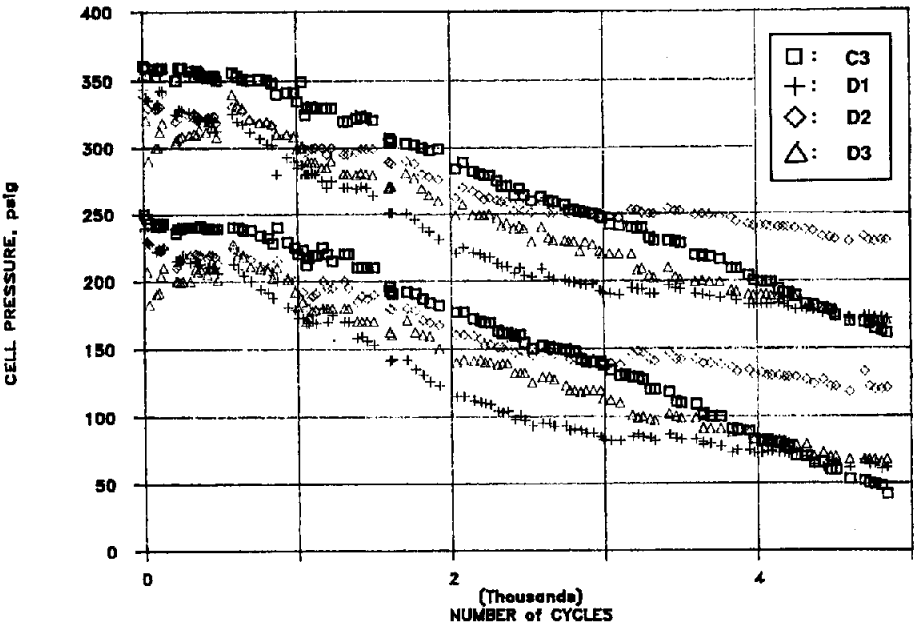


Fig. 5. Plots of end-of-charge pressure (EOCPs) and end-of-discharge pressure (EODPs) vs. number of cycles during the cycling test of C-type (85% porous) and D-type (90% porous electrodes): (□) C3; (+) D1; (◇) D2, and (△) D3.

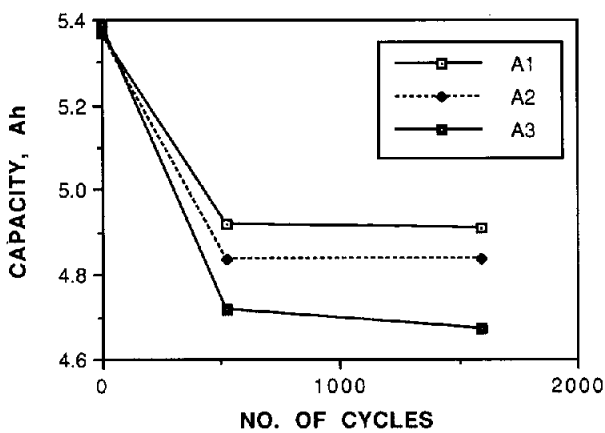


Fig. 6. Plots of interim capacity values of A-type cells (85% porous, 0.8 mm thick electrodes) vs. number of cycles.

*Destructive physical analysis*

All cells were disassembled after post-cycling test for destructive physical analyses (DPA). Cell stacks were inspected visually for physical changes of the cell stacks or components. No sign of a 'soft short' was found in the stack. Physical condition of the cell stacks was good in comparison with those of other long cycled cells [6].

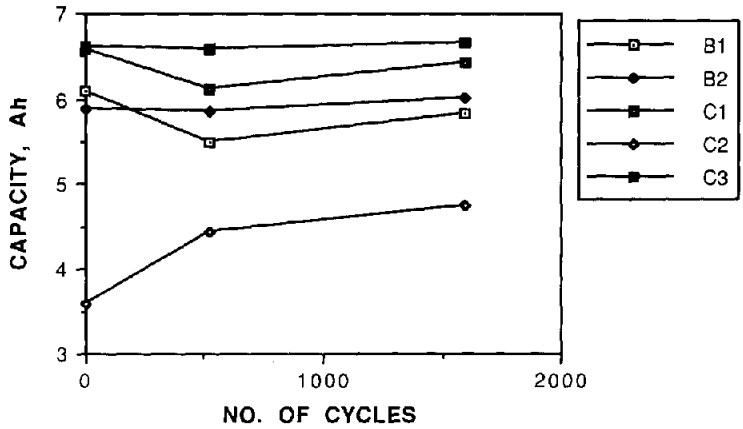


Fig. 7. Interim capacity values of B- and C-type cells (85% porous electrodes) vs. number of cycles.

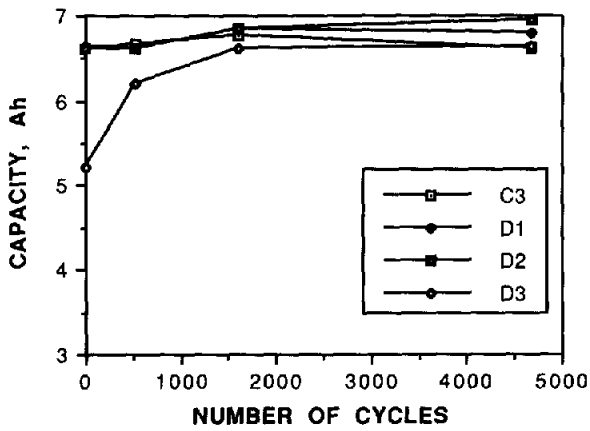


Fig. 8. Interim capacity values of D-type cells (90% porous electrodes) vs. number of cycles.

There was a large population of 'popping' holes in A-type cells which contained 0.8 mm thick electrodes without the polypropylene felt electrolyte reservoir. This population was much higher than those observed in the state-of-the-art individual pressure vessel (IPV) cells using zirconia separators [9]. However, in other type cells which contained 2 mm thick electrodes with the polypropylene felt electrolyte reservoir, the 'popping' hole population was much smaller than in the other cells. The cause of these differences in degree of 'popping' is speculated as follows: in a state-of-the-art IPV cell with conventional nickel electrodes and a 'back-to-back' stack configuration, pores in the nickel electrode are smaller than those in the zirconia separator. Oxygen evolved in the bulk of the nickel electrode should be divided into both sides of the electrode because of the capillary bubble pressure in the pores. As a result of this division, roughly one half of the oxygen will go through the separator causing the 'popping'. The other half may leave the stack through the gap opening between two nickel electrodes. This gap opening is due to the presence of the nickel wire screens on the back side of the electrodes preventing the formation of a tight gas seal between

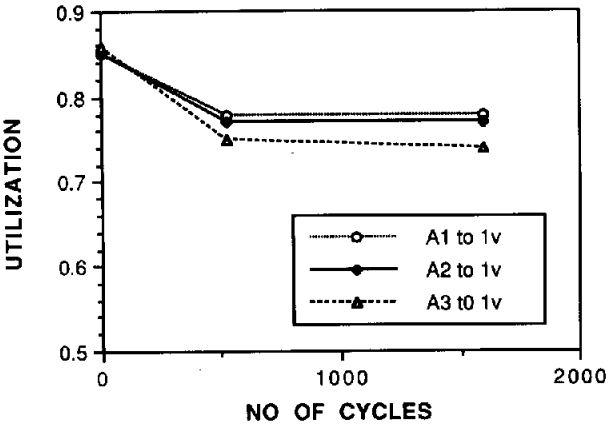


Fig. 9. Utilization values from interim capacity measurements of A-type (85% porous, 0.8 mm thick electrodes) cells vs. number of cycles.

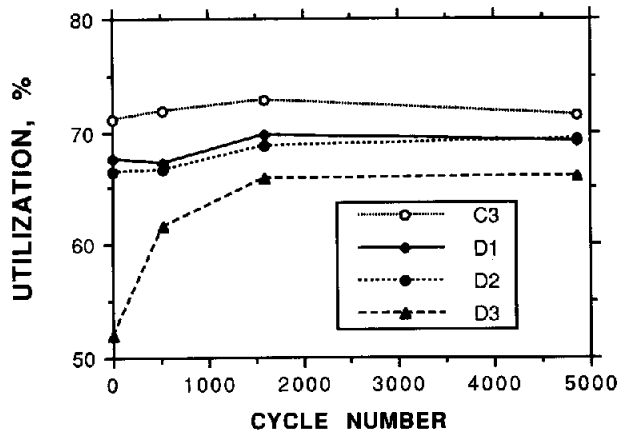


Fig. 10. Utilization values from interim capacity measurements of C-type (85% porous) and D-type (90% porous electrodes) cells vs. number of cycles.

them. However, gaps between two nickel electrodes in A-type cells were tighter than those in the state-of-the-art IPV cells because there are no nickel screens in the present electrodes. Therefore, a good portion of the oxygen which was evolved in the backside of the nickel electrode might have been forced through large pores in the electrodes which were visible when the electrodes were held against a bright light source. This additional oxygen might cause more severe 'popping' in these cells than the state-of-the-art IPV cell. However, in other type (B, C, and D) cells which contain the polypropylene felt electrolyte reservoir, the pores in the reservoir are larger than those in the electrode or the separator. Therefore, most of the evolved oxygen is expected to go out of the stack through the reservoir.

Heavy disintegration of polypropylene felt reservoir material has been observed in many cells (B2, C2, C3, D2, and D3) showing missing areas of the reservoir material. Damage apparently is by chemical or electrochemical disintegration (probably an oxidation). However, the relative degree of disintegration was highly variable showing

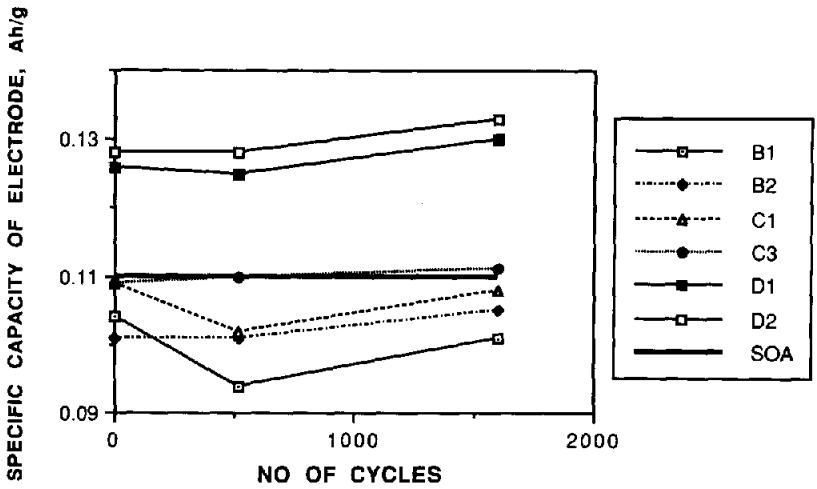


Fig. 11. Specific capacity values of various types of electrodes vs. number of cycles; SOA: state-of-the-art nickel electrode.

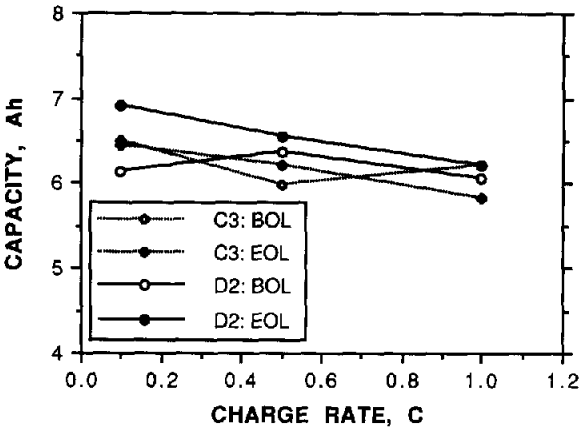


Fig. 12. Effects of charge rates on measured capacity of C-type (85% porous) and D-type (90% porous electrodes) cells before and after the cycling test; BOL: beginning of life, EOL: end of life.

no missing area of the material in some cells (C1, B1, and D1). The cause of such variation is not well understood. The average value of the nickel electrode expansion after 4860 cycles was less than 15% (Table 3). This expansion is moderate compared with those in the state-of-the-art IPV cell [9]. However, there was substantial shedding of loose active material with the cycled electrodes during capacity measurements in flooded electrolyte cells. As a result of such loss of active material, measured values of electrode capacity are highly variable and often smaller than the capacity in the cell as shown in Table 4. Chemical analysis and SEM study of the electrodes are in progress in order to evaluate the utilization of the active material in various KOH concentrations before and after the cycling test.

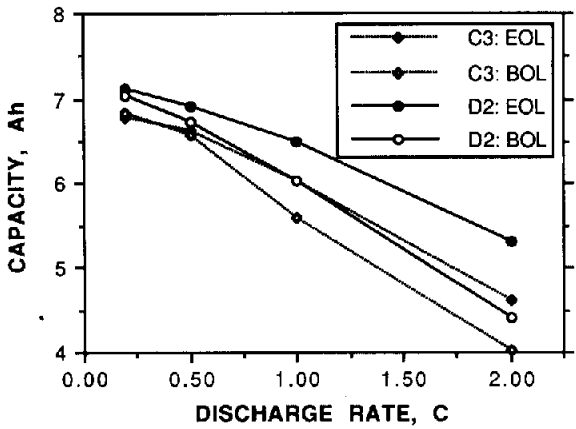


Fig. 13. Effects of discharge rates on measured capacity of C-type (85% porous) and D-type (90% porous electrodes) cells before and after the cycling test; BOL: beginning of life, EOL: end of life.

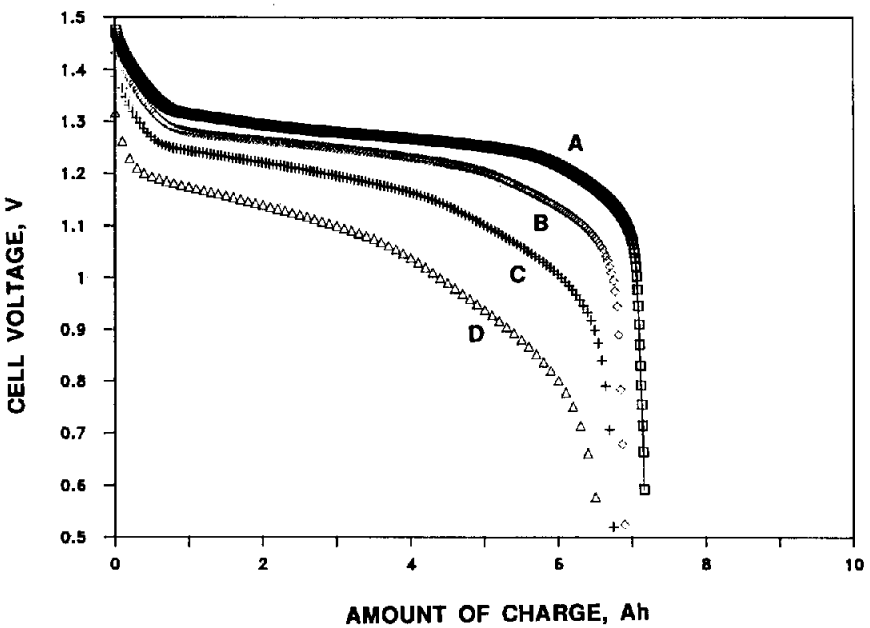


Fig. 14. Discharge voltage curves at various discharge rates of D2 cell before cycling test: (A) at *C*/5 rate; (B) at *C*/2 rate; (C) at *C* rate, and (D) at 2*C* rate.

## Concluding remarks

Nickel electrodes using high porosity 'Fibrex' substrates have substantially improved theoretical capacity over that of state-of-the-art sintered nickel plaque electrodes. However, utilization of the active material was low (65 to 80%) compared with that of the state-of-the-art ones (approximately 90%) in 26% KOH. The observed low

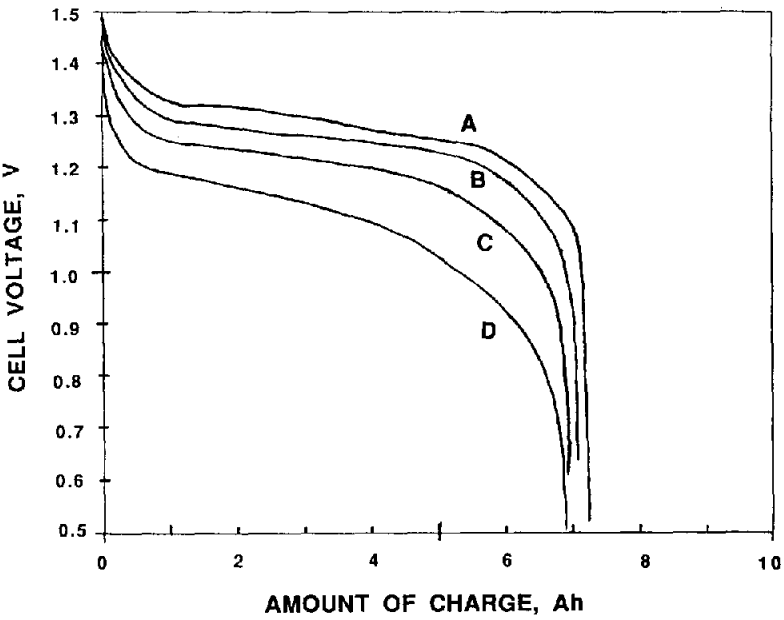


Fig. 15. Discharge voltage curves at various discharge rates of D2 cell after cycling test: (A) at *C*/5 rate; (B) at *C*/2 rate; (C) at *C* rate, and (D) at 2*C* rate.

TABLE 3

Change of electrode thickness after the cycling test

| Cell no. | No. of cycles | Electrode thickness before cycle test (mm) | Electrode thickness after cycle test (mm) | Change (%) |
|---|---|---|---|---|
| A1 | 2354 | 0.810 | 0.995 | 22.8 |
| A2 | 2937 | 0.828 | 0.907 | 9.5 |
| A3 | 2017 | 0.805 | 0.978 | 21.5 |
| B1 | 2011 | 2.251 | 2.302 | 2.3 |
| B2 | 2743 | 2.234 | 2.577 | 15.4 |
| C1 | 2811 | 2.294 | 2.549 | 11.1 |
| C2 | 1813 | 2.212 | 2.445 | 10.5 |
| C3 | 4860 | 2.215 | 2.493 | 12.6 |
| D1 | 4860 | 2.155 | 2.535 | 17.6 |
| D2 | 4860 | 2.155 | 2.522 | 17.0 |
| D3 | 4860 | 2.225 | 2.437 | 9.5 |

utilization of the presently studied electrodes might be due to the presence of large pores as shown in Fig. 1. Due to this low utilization, the electrodes using 85% porous substrates did not show any advantage over the state-of-the-art ones, but the ones using a 90% porous substrate showed 17% higher usable specific capacity (about 0.13 Ah/g in 26% KOH) than that of the state-of-the-art ones. These electrodes achieved up to 4860 cycles at 40% depth-of-discharge with neither capacity loss nor

TABLE 4

Electrode-capacity values in flooded cells with 26, 31, and 36% KOH electrolytes. Charged at *C*/10 rate for 18 h followed by discharge at *C*/2 rate to −1.0 V vs. a nickel sheet counter electrode

| Electrode | In cell[a] (Ah) | Concentration KOH electrolyte | | |
|---|---|---|---|---|
| | | 26% (Ah) | 31% (Ah) | 36% (Ah) |
| C new | | 3.21 | 3.41 | 3.63 |
| C3 | 2.3 | 3.66 | 3.88 | 4.14 |
| D1 | 3.4 | 3.27 | 3.58 | 3.86 |
| D2 | 3.5 | 2.27 | 2.52 | 2.75 |
| D3 | 3.3 | 3.5 | 3.82 | 3.92 |

[a]Prior to destructive physical analyses.

any significant changes of rate capability and charging efficiency with cycling. We plan to investigate these electrodes further to improve the active-material utilization.

## Acknowledgements

This work is supported by a NASA Lewis Research Center (Contract No. NAS 3-22238). The authors would like to thank Mr J. J. Smithrick for valuable technical discussions and Mr D. B. Losee for pre-disassembly capacity measurements.

## References

1 W. U. Borger and L. D. Massie, *Proc. 25th Intersociety Energy Conversion Engineering Conf., Reno, NV, USA, Aug. 1990,* p. 1.
2 H. S. Lim and S. A. Verzwyvelt, *J. Power Sources, 22* (1988) 213.
3 J. J. Smithrick and S. W. Hall, *Proc. 26th Intersociety Energy Conversion Engineering Conf., Boston, MA, USA, Aug. 1991,* Vol. 3, p. 277.
4 D. L. Britton, *Proc. 34th Int. Power Sources Symp., Cherry Hill, NJ, USA, 1990,* p. 236.
5 D. F. Pickett, *Ext. Abstr., The Electrochemical Society Fall Meet., Boston, MA, USA, 1973,* p. 119, Abstr. No. 49.
6 H. S. Lim and S. A. Verzwyvelt, *Proc. 19th Intersociety Energy Conversion Engineering Conf., San Francisco, CA, USA, Aug. 1984,* p. 312.
7 H. S. Lim and S. A. Verzwyvelt, *J. Power Sources, 29* (1990) 503.
8 E. Levy, *Proc. 17th Intersociety Energy Conversion Engineering Conf., Los Angeles, CA, USA, Aug. 1982,* p. 774.
9 H. S. Lim, G. R. Zelter, J. J. Smithrick and S. W. Hall, *Proc. 26th Intersociety Energy Conversion Engineering Conf., Boston, MA, USA, Aug. 1991,* Vol. 3, p. 309.